Journal of Computational Physics 228 (2009) 2535–2551

Contents lists available at ScienceDirect

Journal of Computational Physics

journal homepage: www.elsevier.com/locate/jcp

On computational issues of immersed finite element methods

X. Sheldon Wang [a,*], L.T. Zhang [b], Wing Kam Liu [c]

[a] Department of Mathematical Sciences, New Jersey Institute of Technology, 323 Martin Luther King Jr. Blvd., Newark, NJ 07102, United States
[b] Department of Mechanical, Aerospace, and Nuclear Engineering, Rensselaer Polytechnic Institute, Troy, NY 12180, United States
[c] Department of Mechanical Engineering, Northwestern University, Evanston, IL 60208, United States

ARTICLE INFO

Article history:
Received 4 March 2008
Received in revised form 26 November 2008
Accepted 9 December 2008
Available online 24 December 2008

Keywords:
Fluid–structure interaction
Mixed finite element formulation
Immersed boundary method
Immersed continuum method
Immersed finite element
Driven cavity

ABSTRACT

The objective of this paper is to provide a review of recent finite element formulations for immersed methods. In these finite element formulations, independent Lagrangian solid meshes are introduced to move on top of a background Eulerian fluid mesh. This key feature allows the handling, without excessive fluid mesh adaptation, multiple deformable solids immersed in viscous fluid. In particular, pros and cons of both explicit and implicit approaches are illustrated along with subtle differences between incompressible and slightly compressible models.

Published by Elsevier Inc.

1. Introduction

Numerical investigations of fluid–structure interaction problems require reliable numerical modeling and simulation tools [19,32]. An efficient and robust modeling technique is essential in the study of complicated physical phenomena, especially in bioscience and biomedical fields. In the past few decades, numerous research efforts have been directed to method development for the modeling of fluid–structure interaction systems. Stabilized methods are widely used in the simulation of fluid–particle and fluid–structure interactions [20]. The arbitrary Lagrangian Eulerian (ALE) formulation is commonly introduced to accommodate the complicated fluid–structure interfacial motions [12,31,35]. In general mesh updating and remeshing processes are computationally expensive. Recently, the fictitious domain method and the extended finite element method have been proposed to study fluid–structure interactions [5,10,11].

The immersed boundary method was originally developed by Peskin for the computation of blood flows interacting with the heart and heart valves [6]. The mathematical formulation of the IB method employs a mixture of Eulerian and Lagrangian descriptions for fluid and solid domains. The interaction between fluid and solid domains is accomplished by distributing nodal forces and interpolating nodal velocities between Eulerian fluid and Lagrangian solid domains. The advantage of the IB method is that the fluid–structure interface is automatically tracked, which circumvents costly mesh updating algorithms. One major obstacle of the IB method is the assumption of the fiber-like immersed elastic structure. This assumption restrains realistic modeling of structures that may require complicated constitutive laws and an accurate representation of the finite volume occupied by immersed solids within the fluid domain. Nevertheless, the concept of the IB method had profound impacts. Since the inception of finite element formulations of immersed methods, a wealth of extensions have been

* Corresponding author. Tel.: +1 9735965378l; fax: +1 97359655991.
E-mail address: xwang@njit.edu (X. S. Wang).

0021-9991/$ - see front matter Published by Elsevier Inc.
doi:10.1016/j.jcp.2008.12.012

introduced to connect the immersed finite element method with molecular dynamics and various multi-scale and multi-physics models [9,30]. In the initial attempt to employ finite element formulations with immersed methods, so-called extended immersed boundary method was introduced to represent immerse solids with nonlinear finite element formulations [27]. In this attempt, the fluid solver remains the same as the immersed boundary method and discretized delta functions are still based on uniform background fluid grids. In another attempt, so-called immersed finite element method (IFEM) was developed to represent the background viscous fluid with an unstructured finite element mesh in addition to nonlinear finite elements for immersed solids [34]. In IFEM, kernels of reproduced kernel particle method (RKPM) are employed for unstructured background finite element meshes [29]. This meshfree delta function provides not only a higher order smoothness in coupling fluid and solid domains, but also the ability to handle nonuniform fluid grids, which offers flexibility and robustness in the numerical scheme. However it has been pointed out and confirmed mathematically that as long as the power input to the surrounding fluid is preserved, the communication between two domains can be simply accomplished by finite element interpolation functions within each element [2]. In these earlier finite element based immersed methods, explicit time integration schemes are used. Moreover, because the surrounding viscous fluid is incompressible, the immersed deformable solid is also kept incompressible. In addition, mixed finite element formulations have been introduced to handle compressible solid immersed in compressible viscous fluid [23,24]. With the implicit and compressible finite element formulations, it is anticipated that immersed methods can be directly implemented for various continua immersed in a background continuum. The goal of this paper is to provide a recap of recently activities and to compare explicit with implicit and compressible with incompressible finite element formulations.

2. Immersed incompressible continuum

Instead of representing the immersed structures/solids with fibers, nonlinear finite element formulations are employed in recent immersed finite element methods [27,34]. The initial attempt of connecting a traditional linear elastic model with the immersed boundary method can be traced back to Sulsky and Brackbill [17], in which a stress function is transferred to the fluid grid. In these new attempts, submerged solids can experience large displacements and deformations. If the surrounding fluid is viscous and incompressible, the immersed solid must be incompressible in immersed methods. There are two views of immersed solids. The first one which matches with the original understanding of the immersed boundary method, namely, the immersed solid is wet and permeated with the same fluid as the surrounding. Therefore, the elasticity forces will be the additional force due to the solid portion of the immersed solid. This understanding seems realistic for biological system modeling, since the tissues are mostly fluid–solid systems and the elastic parts are contributed by elastomer, collagen, or other solid constituents. On the other hand, the second understanding of the immersed solid is more in tune with the traditional fluid–structure interaction systems in which the immersed solid is dry and impermeable. If the immersed solids are impermeable, the additional elastic forces are large in comparison with the viscous counterparts calculated with the material properties of the surrounding fluid, both views for immersed solids could yield the same forces.

In the initial versions of finite element formulations for immersed methods [2,27,34], the immersed solids are assumed to be incompressible. Detailed convergence studies have also been presented in Ref. [3,4]. Consider a general three-dimensional incompressible hyperelastic material model with the following Mooney–Rivlin material description

$$W = C_1(J_1 - 3) + C_2(J_2 - 3), \tag{2.1}$$

with

$$J_1 = I_1, \quad J_2 = I_2, \quad I_1 = C_{kk}, \quad I_2 = (I_1^2 - C_{ij}C_{ij})/2, \tag{2.2}$$

where W is the elastic energy potential and $\mathbf{C}$ is the Cauchy–Green deformation tensor defined as $\mathbf{C} = \mathbf{D}^T\mathbf{D}$ with the solid deformation gradient $D_{ij} = \partial x_i^s(t)/\partial x_j^s(0)$.

Note that since the solid displacements are mapped from the background fluid, if the surrounding fluid is incompressible, the solid must also be incompressible, which corresponds to $J_3 = I_3^{1/2} = (det(\mathbf{C}))^{1/2} = 1$. However, no additional measures are taken to enforce such a constraint which might pose a problem for the volume conservation of the immersed solid. For structures with large displacements and deformations, the second Piola–Kirchhoff stress $\mathbf{S}$ and the Green–Lagrangian strain ϵ are used along with a total Lagrangian formulation. Hence, employing Eq. (2.1), we derive

$$S_{kl} = \frac{\partial W}{\partial \epsilon_{kl}} \quad \text{and} \quad \epsilon_{ij} = \frac{1}{2}(C_{ij} - \delta_{ij}). \tag{2.3}$$

Thus, the equivalent internal force for the material points of the flexible structure can be derived as

$$\mathbf{F}_k = \frac{\partial}{\partial \mathbf{x}_k^s}\left(\int_{\Omega_s(t)} W d\Omega\right) = \int_{\Omega_s(0)} S_{ml}\frac{\partial \epsilon_{ml}}{\partial \mathbf{x}_k^s} d\Omega, \tag{2.4}$$

where $\mathbf{x}_k^s$ and $\mathbf{F}_k$ stand for the current position vector of the kth submerged node and the corresponding internal nodal force vector, respectively, and $\Omega_s(t)$ and $\Omega_s(0)$ represent the current and the original volume of the submerged solid.

Note that if the nonlinear structural material has a density ρ_s different from the fluid density ρ_f, we should also include the inertial force. Consequently, the resultant node force vector $\mathbf{R}$, a combination of the surrounding fluid force $\mathbf{R}^f$ and other external force $\mathbf{R}^e$, can be expressed for each material point:

$$\mathbf{R} = \mathbf{R}^f + \mathbf{R}^e = \begin{cases} \mathbf{F}, & \rho_s = \rho_f, \\ \mathbf{F} + \mathbf{M}\ddot{\mathbf{U}}, & \rho_s \neq \rho_f, \end{cases} \tag{2.5}$$

where $\mathbf{U}$ represents the nodal displacement vector and the consistent mass matrix $\mathbf{M}$ is defined as

$$\mathbf{M} = \int_{\Omega_s(0)} (\rho_s - \rho_f)\mathbf{H}^T\mathbf{H}\det(\mathbf{D})d\Omega, \tag{2.6}$$

with $\mathbf{H}$ as the interpolation matrix.

Based on the concept of immersed methods, it is the force $\mathbf{R}^f$ that we must distribute to the surrounding fluid. Finally in explicit schemes, we have

$$\mathbf{f} = -\int_{\Omega_s(t)} \mathbf{R}^f \delta(\mathbf{x} - \mathbf{x}^s)d\Omega, \tag{2.7}$$

$$\mathbf{R}^f = \int_{\Omega_s(0)} \mathbf{S}\frac{\partial \epsilon}{\partial \mathbf{x}^s}d\Omega + \int_{\Omega_s(0)} (\rho_s - \rho_f)\mathbf{H}^T\mathbf{H}\det(\mathbf{D})d\Omega\ddot{\mathbf{U}} - \mathbf{R}^e, \tag{2.8}$$

$$\mathbf{v}^s = \int_{\Omega} \mathbf{v}\delta(\mathbf{x} - \mathbf{x}^s)d\Omega, \tag{2.9}$$

where $\Omega_s(0)$ represents the original solid configuration employed in the total Lagrangian formulation.

Eq. (2.8) is used to derive nodal forces attached to immersed solid material points; Eq. (2.7) is employed to distribute the nodal forces to the surrounding fluid; and Eq. (2.9) is applied to interpolate the velocity of the solid node based on the velocities of the surrounding fluid nodes. Notice that Eq. (2.7) is carried out in the current configuration of the submerged solid and the same kernel is used in Eqs. (2.7) and (2.9).

3. Immersed compressible continuum

In the case of incompressible solid immersed in incompressible fluid, if there is no excessively stiff boundary springs connecting with tether points and the additional elasticity moduli of the immersed solid are reasonable, the traditional explicit scheme can be employed [27,34]. In this section, we discuss a general case of compressible solid immersed in compressible fluid. In fact, this general case also covers one seemingly very different scenario, namely, compressible solid immersed in incompressible fluid. In the immersed continuum method, we use a physical argument such that the bulk modulus of the solid can be much higher than the bulk modulus of the fluid. With the assumption that the acoustic wave speed within the fluid is constant, a so-called pseudo compressible fluid model is often used in numerics to mimic incompressible fluid behaviors. However, since this model is the same as isentropic acoustic fluid and fluid–structure interaction systems [26], with sufficiently small time steps, pressure wave propagation and related scattering and radiation phenomena will be captured. The traditional assumption for acoustic FSI systems is small strain and small displacement, namely, the FSI interface does not move at all. It seems that immersed methods bear no advantages over traditional mixed finite element formulations or potential formulations [25]. Why do we have to bother with this type of fluid model coupled with compressible solid? First of all, there will be cases where pressure waves are strong enough to move the immersed solid. Secondly, to use the concept of immersed methods, we need to replace the immersed solid with a fluid the same as the surrounding fluid. If the volume of the immersed solid changes ever so slightly, the volume of the corresponding fluid must also change, hence, the model of the surrounding fluid must also be slightly compressible. Of course, it is possible that with sufficiently large time steps in the implicit time integration procedures, the pressure waves due to volumetric changes will not be captured accurately, however the transient behaviors of fluid–structure interactions due to inertial and viscosity will be accurately depicted. It is important to point out that here the immersed solid is viewed as impermeable thus such a volume of fluid does not exist physically. To account for the correct effect of the submerged solid exerting on the surrounding fluid, we must subtract the inertial force, the external body force, and the internal stress effects of such an imaginary fluid volume $\Omega_s(t)$. This idea is similar to the fictitious domain method [11,22,33]. The key difference is that the displacement unknowns of the immersed solids are not considered as part of the independent unknowns. If they are listed as independent variables along with the corresponding Lagrangian multipliers, the immersed boundary/continuum methods and the fictitious domain method might share the same inf-sup condition similar to the modeling of almost incompressible materials [1].

Consider the same domain Ω, suppose there exists a submerged solid domain Ω_s enclosed by a sufficiently smooth boundary Γ_s, the entire domain Ω is subdivided into two regions, namely, the solid region Ω_s and the fluid region Ω_f. Therefore, the boundaries of the solid and the fluid regions can be simply expressed as $\partial\Omega_s = \Gamma_s$ and $\partial\Omega_f = \Gamma_s \cup \Gamma_v \cup \Gamma_f$. Denote $\boldsymbol{\sigma}$ as the stress tensor, $\mathbf{v}$ as the velocity vector, we establish the following set of governing equations (strong form):

$$\rho_s \dot{v}_i^s = \sigma_{ij,j}^s + \rho_s g_i, \quad \text{in} \quad \Omega_s, \tag{3.10}$$

$$\rho_f \dot{v}_i^f = \sigma_{ij,j}^f + \rho_f g_i, \quad \text{in} \quad \Omega_f, \tag{3.11}$$

$$[v_i] = 0, \quad \text{on} \quad \Gamma_s, \quad \text{kinematic matching}, \tag{3.12}$$

$$[\sigma_{ij} n_j] = 0, \quad \text{on} \quad \Gamma_s, \quad \text{dynamic matching}, \tag{3.13}$$

where the surface normal vector $\mathbf{n}$ is aligned with that of the solid domain $\mathbf{n}^s$ and opposite to that of the fluid domain $\mathbf{n}^f$.

Define the same Sobolev space $[H^1_{0,\Gamma_v}(\Omega)]^d$, we express Eqs. (3.10)–(3.13) in the variational form (weak form): $\forall \mathbf{w} \in [H^1_{0,\Gamma_v}(\Omega)]^d$

$$\int_{\Omega_s} w_i \left[\rho_s(\dot{v}_i^s - g_i) - \sigma_{ij,j}^s\right] d\Omega + \int_{\Omega_f} w_i \left[\rho_f\left(\dot{v}_i^f - g_i\right) - \sigma_{ij,j}^f\right] d\Omega = 0. \tag{3.14}$$

Again, using integration by parts and the divergence theorem, introducing dynamic matching at the interface Γ_s, and combining the solid and fluid domains with $\Omega_s \cup \Omega_f = \Omega$, Eq. (3.14) can be rewritten as: $\forall \mathbf{w} \in \left[H^1_{0,\Gamma_v}(\Omega)\right]^d$

$$\int_{\Omega} [w_i \rho_f(\dot{v}_i - g_i) + w_{i,j}\sigma_{ij}] d\Omega - \int_{\Gamma_f} w_i f_i^{\Gamma_f} d\Gamma - \int_{\Omega_s} w_i^s f_i^s d\Omega = 0, \tag{3.15}$$

with

$$\int_{\Omega_s} w_i^s f_i^s d\Omega = -\int_{\Omega_s} \left[w_i(\rho_s - \rho_f)(\dot{v}_i - g_i) + w_{i,j}\left(\sigma_{ij}^s - \sigma_{ij}^f\right)\right] d\Omega. \tag{3.16}$$

In the explicit implementation, we introduce the following two key equations to synchronize the fluid occupying the submerged solid domain Ω_s with the solid:

$$f_i^{fsi} = \int_{\Omega_s} f_i^s \delta(\mathbf{x} - \mathbf{x}^s) d\Omega, \tag{3.17}$$

$$v_i^s = \int_{\Omega} v_i \delta(\mathbf{x} - \mathbf{x}^s) d\Omega, \tag{3.18}$$

where $\mathbf{f}^{fsi}$ represents the same equivalent body force as in the immersed boundary method.

It is very important to recognize that $\mathbf{f}^s$ is the force density within the solid domain Ω_s; whereas $\mathbf{f}^{fsi}$ is the equivalent body force over the entire domain Ω. In fact, $\mathbf{f}^s$ can be viewed as the Lagrangian multiplier for the constraint $\mathbf{v}^f = \mathbf{v}^s$ within the solid domain Ω_s.

For the fluid domain, we adopt an Eulerian kinematic description and for convenience omit the superscript f, therefore, the material derivative of the fluid velocity is expressed as

$$\dot{v}_i = v_{i,t} + v_j v_{i,j}. \tag{3.19}$$

For the solid domain, we employ a Lagrangian kinematic description, thus the fluid–solid interface will be tracked automatically by the position of solid particles. Moreover, there is no need for convective terms in the solid domain and the material derivative is the same as the time derivative. Hence, the solid velocity vector $\mathbf{v}^s$ and the acceleration vector $\dot{\mathbf{v}}^s$ can be expressed as

$$\mathbf{v}^s = \dot{\mathbf{u}}^s \quad \text{and} \quad \dot{\mathbf{v}}^s = \ddot{\mathbf{u}}^s, \tag{3.20}$$

with the displacement vector $\mathbf{u}^s(t) = \mathbf{x}^s(t) - \mathbf{x}^s(0)$, where $\mathbf{x}^s(t)$ and $\mathbf{x}^s(0)$ stand for the current and the original material point positions within the solid domain Ω_s.

In order to deal with the compressible viscous fluid, we subtract the pressure p from the stress components σ_{ij} and obtain the deviatoric stress components τ_{ij}, which is illustrated in a Newtonian fluid model,

$$\sigma_{ij} = -p\delta_{ij} + \tau_{ij}, \tag{3.21}$$

with $\tau_{ij} = \mu(v_{j,i} + v_{i,j})$.

Furthermore, to couple with the pressure unknown, the continuity equation of the compressible viscous fluid is expressed as

$$v_{i,i} + \frac{\dot{p}}{\kappa} = 0, \tag{3.22}$$

where κ is the bulk modulus of the fluid and the material derivative $\dot{p}$ can be simply expressed as $p_{,t} + v_i p_{,i}$ for the Eulerian description.

In the analysis of slightly compressible fluids, we assume the compressibility measured by bulk modulus κ is constant. Therefore, we have the following relationship between the density and the pressure of the fluid domain,

$$\frac{dp}{d\rho} = c^2 = \frac{\kappa}{\rho}. \tag{3.23}$$

From Eq. (3.23), it is straightforward to derive the following

$$p(t) - p(0) = \kappa \ln \frac{\rho(t)}{\rho(0)}. \tag{3.24}$$

Like the fluid stress tensor, we also decompose the solid stress tensor as a hydrostatic pressure p^s, and a deviatoric stress tensor τ^s_{ij},

$$\sigma^s_{ij} = -p^s \delta_{ij} + \tau^s_{ij}. \tag{3.25}$$

In order to extend the incompressible nonlinear solid model to compressible model, as discussed in Ref. [18], we introduce

$$\bar{W} = C_1(J_1 - 3) + C_2(J_2 - 3) + \kappa^s (J_3 - 1)^2/2, \tag{3.26}$$

along with an additional elastic energy term $-[p^s + \kappa^s(J_3 - 1)]^2/2\kappa^s$ to $\overline{W}$.

Therefore, the continuity equation becomes a constraint for the solid unknown pressure p^s

$$J_3 - 1 + \frac{p^s}{\kappa^s} = 0, \tag{3.27}$$

where κ^s is the solid bulk modulus and J_3 stands for the determinant of the deformation gradient $\mathbf{D}$.

Of course, the solid Cauchy stress can be converted from the second Piola–Kirchhoff stress,

$$\sigma^s_{ij} = \frac{1}{J_3} D_{im} S_{mn} D_{jn}. \tag{3.28}$$

Finally, since the solid displacement is dependent on the fluid velocity, the primary unknowns for the coupled fluid–solid system are the fluid velocity $\mathbf{v}$, the fluid pressure p, and the solid pressure p^s. Define the Sobolev spaces, so the weak form of governing equations can be modified as: $\forall q \in L^2(\Omega)$, $q^s \in L^2(\Omega_s)$, $\mathbf{w} \in [H^1_{0,\Gamma_v}(\Omega)]^d$, which includes $\forall \mathbf{w}^s \in [H^1(\Omega_s)]^d$, and find $\mathbf{v}$ and p in Ω, p^s in Ω_s, such that

$$\begin{aligned}
&\int_\Omega w_i \rho(\dot{v}_i - g_i) d\Omega + \int_\Omega (w_{i,j}\tau_{ij} - p w_{i,i}) d\Omega - \int_{\Gamma_f} w_i f_i^{\Gamma_f} d\Gamma + \int_{\Omega_s} \left[w^s_i(\rho_s - \rho)(\dot{v}_i - g_i) + w^s_{i,j}\left(\tau^s_{ij} - \tau^f_{ij}\right) - (p^s - p) w^s_{i,i} \right] d\Omega \\
&\quad + \int_\Omega q\left(v_{j,j} + \frac{p_{,t}}{\kappa}\right) d\Omega + \int_{\Omega_s} q^s \left(J_3 - 1 + \frac{p^s}{\kappa^s}\right) d\Omega = 0.
\end{aligned} \tag{3.29}$$

We recognize that there are two sets of discretizations, namely, one for the Lagrangian solid mesh and the other one for the Eulerian fluid mesh. Note that the convective terms are hidden in $\dot{v}^h_i$ and the detailed expressions of other stabilized Galerkin formulation for the Navier–Stokes equations can also be found in Refs. [20,21]. In general the interpolation functions for the velocity vector and the unknown pressures are different. Therefore, we retain the superscripts v and p to denote such differences. For the fluid domain Ω, the following interpolations are used:

$$\mathbf{v}^h = h^v_I \mathbf{v}_I, \quad \mathbf{w}^h = h^v_I \mathbf{w}_I, \quad p^h = h^p_I p_I, \quad q^h = h^p_I q_I, \tag{3.30}$$

where h^v_I and h^p_I stand for the interpolation functions at node I for the velocity vector and the pressure; and $\mathbf{v}_I$, $\mathbf{w}_I$, p_I, and q_I are the nodal values of the discretized velocity vector, admissible velocity variation, pressure, and pressure variation, respectively.

For the solid domain Ω_s, the discretization is based on the following:

$$\mathbf{u}^{s,h} = h^u_J \mathbf{u}^s_J, \quad \mathbf{w}^{s,h} = h^u_J \mathbf{w}^s_J, \quad p^{s,h} = h^{p^s}_J p^s_J, \quad q^{s,h} = h^{p^s}_J q^s_J, \tag{3.31}$$

where h^u_J and $h^{p^s}_J$ stand for the interpolation functions at node J for the displacement vector and the unknown pressures; and $\mathbf{u}^{s,h}_J$, $\mathbf{w}^{s,h}_J$, $p^{s,h}_J$, and $q^{s,h}_J$ are the nodal values of the discretized displacement vector, admissible velocity variation, pressure, and pressure variation, respectively.

Substituting both discretizations (3.30) and (3.31) into Eq. (3.29), we obtain the following discretization of the weak form: $\forall q^h \in L^2(\Omega^h)$, $q^{s,h} \in L^2(\Omega^h_s)$, $\mathbf{w}^h \in \left[H^{1,h}_{0,\Gamma^h_v}(\Omega^h)\right]^d$, which includes $\forall \mathbf{w}^{s,h} \in \left[H^{1,h}(\Omega^h_s)\right]^d$,

$$\begin{aligned}
&\int_{\Omega^h} w_{il} h^v_I \rho \dot{v}^h_i d\Omega - \int_{\Gamma^h_f} w_{il} h^v_I f_i^{\Gamma^h_f} d\Gamma + \int_{\Omega^h} (w_{il} h^v_{I,j} \tau_{ij} - p^h w_{il} h^v_{I,i}) d\Omega + \int_{\Omega^h_s} [w^s_{ij} h^u_J (\rho_s - \rho)(\dot{v}^h_i - g_i) + w^s_{ij} h^u_{J,j} (\sigma^s_{ij} - \sigma^f_{ij})] d\Omega \\
&\quad - \int_{\Omega^h} w_{il} h^v_I \rho g_i d\Omega + \int_{\Omega^h} q_I h^p_I \left(v^h_{j,j} + \frac{p^h_{,t}}{\kappa}\right) d\Omega + \int_{\Omega^h_s} q^s_J h^{p^s}_J \left(J_3 - 1 + \frac{p^{s,h}}{\kappa^s}\right) d\Omega = 0.
\end{aligned} \tag{3.32}$$

For clarity, we introduce a displacement nodal unknown vector $\mathbf{U}$, although it is only evaluated in the solid domain Ω_s in which a Lagrangian description is prescribed. In fact, within the solid domain, $\mathbf{U}$ is denoted as $\mathbf{U}^s$ and evolves according to $\dot{\mathbf{U}}^s$ and $\ddot{\mathbf{U}}^s$ which are mapped from the velocity nodal unknown vector $\mathbf{V}$ and acceleration nodal unknown vectors $\dot{\mathbf{V}}$ for the fluid domain. Mathematically, we could say that $\mathbf{v}^s$ is $\mathbf{v}$ directly evaluated at the material point $\mathbf{x}^s$. Likewise, the pressure nodal unknown vectors $\mathbf{P}$ and $\mathbf{P}^s$ are introduced for fluid and solid domains, respectively. In this paper, for simplicity, we

employ the Newton–Raphson iteration, and apply the Newmark time integration scheme. For a typical state variable a, in the incremental analysis, we have

$$\begin{aligned} a(t+\Delta t) &= a(t) + \dot{a}(t)\Delta t + [(0.5-\alpha)\ddot{a}(t) + \alpha\ddot{a}(t+\Delta t)]\Delta t^2, \\ \dot{a}(t+\Delta t) &= \dot{a}(t) + [(1-\beta)\ddot{a}(t) + \beta\ddot{a}(t+\Delta t)]\Delta t, \end{aligned} \tag{3.33}$$

where the unknown a stands for the scalar components of the nodal or discretized variables for $\mathbf{V}$, $\mathbf{P}$, and $\mathbf{P}^s$, and α and β are selected integration constants.

At a typical solid node J, with a finite support domain Ω_J, the discretized form of the constraint of the velocities of the immersed solid and the corresponding fluid occupying the same solid domain can be expressed as

$$\mathbf{v}_J^s = \sum_I \mathbf{v}_I \phi_I(\mathbf{x}_I - \mathbf{x}_J^s), \quad \forall \mathbf{x}_I \in \Omega_J, \tag{3.34}$$

where $\phi_I(\mathbf{x}_I - \mathbf{x}_J)$ is the kernel function centered at the solid node J, represented with $\mathbf{x}_J^s$.

Note that in general within the solid domain, we have the stress difference $\sigma_{ij}^s - \sigma_{ij}^f$ or $-(p^s - p^f)\delta_{ij} + \left(\tau_{ij}^s - \tau_{ij}^f\right)$, in addition to the mapping of the velocity vector in Eq. (3.34). In order to use the definition of σ_{ij}^f, we must also map the unknown pressure from the fluid mesh denoted with node I to the solid mesh denoted with node J. In this case, it is beneficial to use the continuous pressure mixed finite element formulation for both fluid and solid domains [1]. Consequently, like Eq. (3.34), we have

$$p_J^f = \sum_I p_I \phi_I(\mathbf{x}_I - \mathbf{x}_J^s), \quad \forall \mathbf{x}_I \in \Omega_J. \tag{3.35}$$

Finally, for the entire domain Ω, due to the arbitrariness of the variations w_{iI}, q_I, and q_J^s, we have four equations at each fluid node I and one equation at each solid node J,

$$r_{iI}^v = 0, \quad r_I^p = 0, \quad r_J^{p^s} = 0, \tag{3.36}$$

where the residuals are defined as

$$\begin{aligned} r_{iI}^v &= \int_{\Omega^h} h_I^v \rho \dot{v}_i^h d\Omega + \int_{\Omega^h} \left[h_{I,j}^v \tau_{ij} - p^h h_{I,i}^v\right] d\Omega - \int_{\Gamma_f^h} h_I^{v,\Gamma_f^h} f_i^{\Gamma_f^h} d\Gamma \\ &\quad + \int_{\Omega_s^h} \mathcal{M}\left[h_J^u(\rho_s - \rho)(\dot{v}_i^h - g_i) + h_{J,j}^u\left(\sigma_{ij}^s - \sigma_{ij}^f\right)\right] d\Omega - \int_{\Omega^h} h_I^v \rho g_i d\Omega, \\ r_I^p &= \int_{\Omega^h} h_I^p \left(v_{j,j}^h + \frac{p_{,t}^h}{\kappa}\right) d\Omega, \quad r_J^{p^s} = \int_{\Omega_s^h} h_J^{p^s} \left(J_3 - 1 + \frac{p^{s,h}}{\kappa^s}\right) d\Omega. \end{aligned} \tag{3.37}$$

At every time step, the nonlinear residual equations in Eq. (3.36) can also be written as follows

$$\mathbf{r}(\mathbf{V}, \mathbf{P}, \mathbf{P}^s) = \mathbf{0}. \tag{3.38}$$

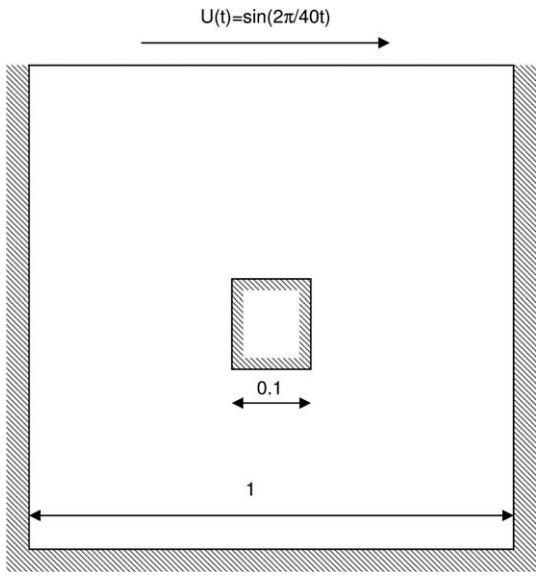

Fig. 1. A driven cavity FSI model with an immersed solid fixed in the center of the cavity.

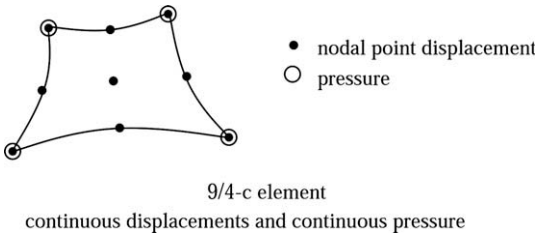

Fig. 2. An illustration of displacement/pressure mixed finite element for solid. The velocity/pressure mixed finite element for fluid has the same arrangement.

4. Matrix-free Newton–Krylov

Recently implicit immersed boundary methods have been studied by Newren et al. [8] in the context of finite difference methods. In this paper, we employ a matrix-free Newton–Krylov iterative procedure for nonlinear sets of Eq. (3.38). In the kth Newton–Raphson iteration at time step $m+1$ of the nonlinear residual Eq. (3.38), from $\mathbf{R}^N$ to $\mathbf{R}^N$, with N as the number of the total unknowns, we start with a first guess of the incremental unknowns $\Delta\mathbf{\Theta}^{k,0}$, namely, $\Delta\mathbf{V}^0$, $\Delta\mathbf{P}^0$, and $\Delta\mathbf{P}^{s,0}$, which often are zero vectors. Then the residual of the linearized systems of equations at the kth Newton–Raphson iteration is evaluated as

$$\mathbf{p} = -\mathbf{r}^{m+1,k-1} - \mathbf{r}_{,v}^{m+1,k-1}\Delta\mathbf{V}^0 - \mathbf{r}_{,p}^{m+1,k-1}\Delta\mathbf{P}^0 - \mathbf{r}_{,p^s}^{m+1,k-1}\Delta\mathbf{P}^{s,0}. \tag{4.39}$$

This error vector is used to construct the n-dimensional Krylov subspace $\mathbf{K}^n$ where $\mathbf{J}$ is the $N \times N$ Jacobian matrix evaluated at time step $m+1$ and the kth Newton–Raphson iteration of the nonlinear residual Eq. (3.38) and can be rewritten as

$$\mathbf{J} = \left(\mathbf{r}_{,v}^{m+1,k-1}, \mathbf{r}_{,p}^{m+1,k-1}, \mathbf{r}_{,p^s}^{m+1,k-1}\right). \tag{4.40}$$

The approximate solution $\Delta\mathbf{\Theta}$ is written as the combination of the initial guess $\Delta\mathbf{\Theta}^{k,0}$ and $\mathbf{z}^n$, with $\mathbf{z}^n \in \mathbf{K}^n$. Note that the dimension of the subspace $\mathbf{K}^n$ is n which is much smaller than the dimension N of the unknown vector $\Delta\mathbf{\Theta}$. The N-dimensional unknown vector $\Delta\mathbf{\Theta}$ or rather $\mathbf{z}^n$ is represented with $\mathbf{V}_n\mathbf{y}$, where $\mathbf{y}$ is a much smaller n-dimensional unknown vector. In the generalized minimum residual (GMRES) method, the modified Gram-Schmidt orthogonalization procedures are used to derive a set of orthonormal vectors v_i, with $1 \le i \le n$ in the Krylov subspace $\mathbf{K}^n$ and an $(n+1) \times n$ upper Hessenberg matrix $\bar{\mathbf{H}}_n$. Define $\mathbf{V}_n = (\mathbf{v}_1\mathbf{v}_2 \ldots \mathbf{v}_n)$ and $\mathbf{V}_{n+1} = (\mathbf{v}_1\mathbf{v}_2 \ldots \mathbf{v}_{n+1})$, we have the following

$$\mathbf{J}\mathbf{V}_n = \mathbf{V}_{n+1}\bar{\mathbf{H}}_n. \tag{4.41}$$

The remaining process in the GMRES method is to solve the least square problem

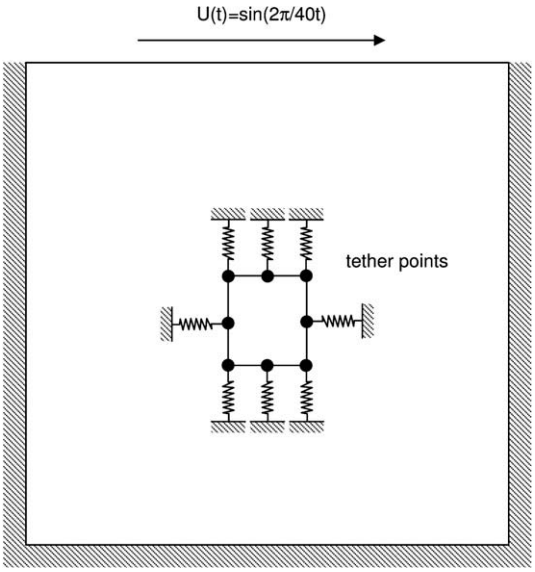

Fig. 3. A driven cavity FSI model with an immersed solid tethered around its boundary points.

$$\min_{\mathbf{z}\in\mathbf{K}^n} \|\mathbf{p}-\mathbf{J}\mathbf{z}\| \text{or} \min_{\mathbf{y}\in\mathbf{R}^n} \|\mathbf{p}-\mathbf{J}\mathbf{V}_n\mathbf{y}\|. \tag{4.42}$$

Assume γ is the length of the initial residual vector $\mathbf{p}$ and $\mathbf{e}_1$ is the unit vector representing the first column of $(n+1)\times(n+1)$ identity matrix, substituting Eq. (4.41), we can show that Eq. (4.42) is equivalent to the following minimization within a much smaller space

$$\min_{\mathbf{y}\in\mathbf{R}^n} \|\gamma\mathbf{e}_1 - \bar{\mathbf{H}}_n\mathbf{y}\|. \tag{4.43}$$

In the matrix-free Newton–Krylov iteration, we do not form the Jacobian matrix. In general, this Jacobian matrix in the immersed boundary/continuum methods has an $O(n^2)$ storage requirement. For large systems with million degrees of freedoms, this Jacobian matrix requires a terabyte (10^{12}) memory which is beyond the limit of computational facilitates available for most scientific researches. It is based on this understanding, we would also like to design a preconditioning technique without the use of the Jacobian matrix [7,13,16].

First of all, the initial residual vector $\mathbf{p}$ in the kth Newton–Raphson iteration at time step $m+1$ of the nonlinear residual Eq. (3.38) is normalized as $\mathbf{v}_1$ with the length $\gamma = \|\mathbf{p}\|_2$. Using Eq. (4.43), we have the corresponding n dimensional residual vector $\mathbf{b} = \gamma\mathbf{e}_1$. Introduce a preconditioning matrix $\mathbf{\Lambda}$, for $i = 1$ to n, using the modified Gram–Schmidt orthogonalization process, we have $\mathbf{q}_i = \mathbf{\Lambda}^{-1}\mathbf{v}_i$ and $\mathbf{w} = \mathbf{J}\mathbf{q}_i$, and for $j = 1$ to$i$, we have $h_{ji} = \mathbf{w}^T\mathbf{v}_j$ and $\mathbf{w}$ is updated with $\mathbf{w} - h_{ji}\mathbf{v}_j$. As a consequence, we obtain $h_{(i+1)i} = \|\mathbf{w}\|_2$ and $\mathbf{v}_{i+1} = \mathbf{w}/h_{(i+1)i}$.

An important procedure in the matrix-free Newton–Krylov is to replace $\mathbf{w} = \mathbf{J}\mathbf{q}_i$ with a finite difference based calculation,

$$\mathbf{J}\mathbf{q}_i \simeq \frac{\mathbf{r}(\mathbf{\Theta}^{m+1,k-1} + e\mathbf{q}_i) - \mathbf{r}(\mathbf{\Theta}^{m+1,k-1})}{e}, \tag{4.44}$$

where e is often set to be around the square root of the machine error [7].

After we establish the elements of an upper $n\times n$ Hessenberg matrix $\mathbf{H}_n$ as well as an upper $(n+1)\times n$ Hessenberg matrix $\bar{\mathbf{H}}_n$, for $j = 1$ to n, and $i = 1$ to $j-1$, a factorization of $\mathbf{H}_n$ is carried out through the following rotation matrix operations,

$$\begin{aligned} h_{ij} &= c_i h_{ij} + s_i h_{(i+1)j}, \\ h_{(i+1)j} &= -s_i h_{ij} + c_i h_{(i+1)j}, \end{aligned} \tag{4.45}$$

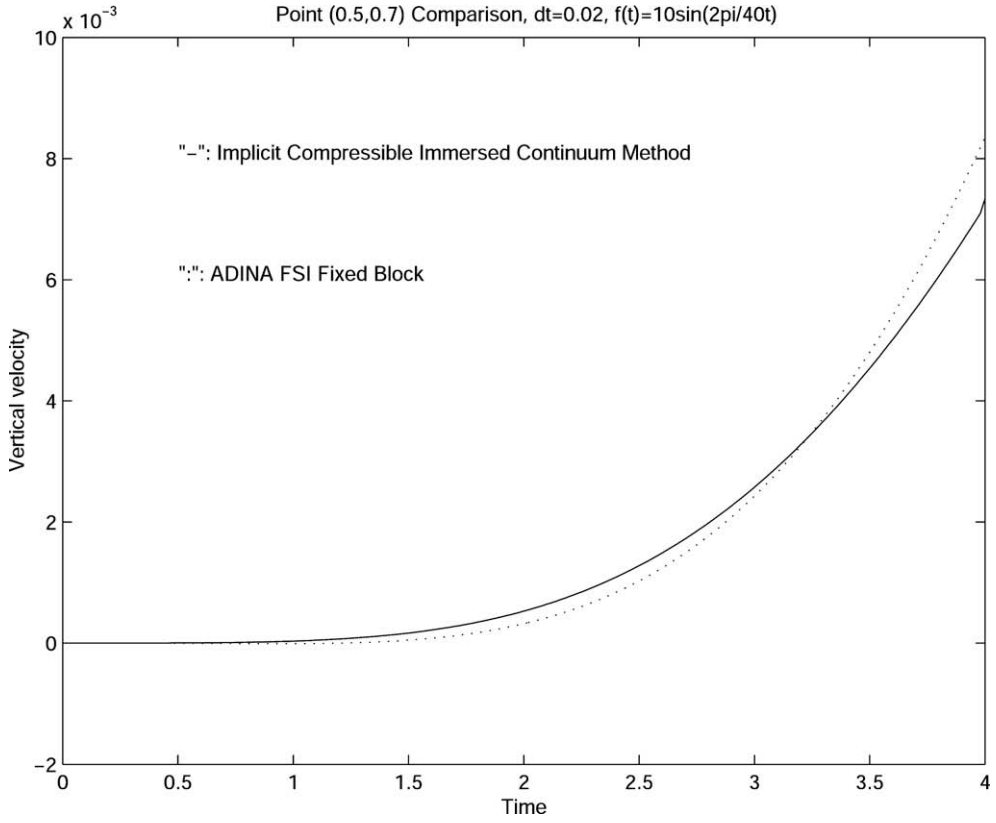

Fig. 4. Horizontal velocity comparison with ADINA FSI.

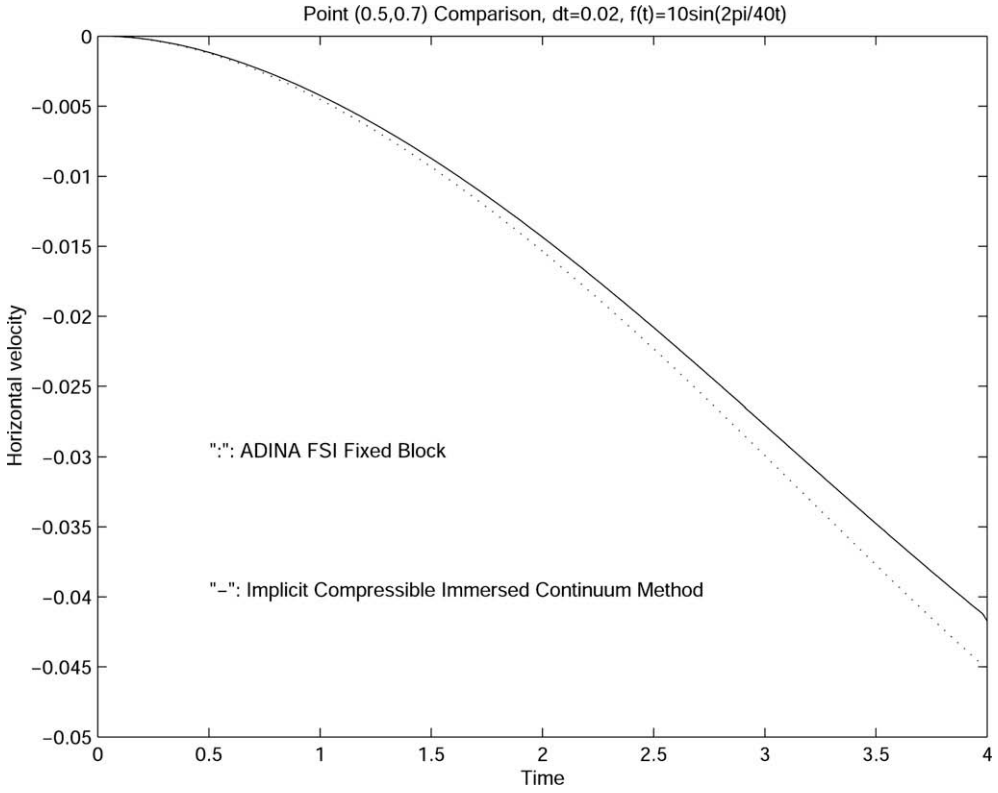

Fig. 5. Vertical velocity comparison with ADINA FSI.

where the entities of the rotation processes are calculated as

$$r = \sqrt{h_{jj}^2 + h_{(j+1)j}^2}, \quad c_j = h_{jj}/r, \quad \text{and} \quad s_j = h_{(j+1)j}/r. \tag{4.46}$$

Through this rotation process, the upper Hessenberg matrix is converted to a diagonal matrix with the coefficients defined as: for $j = 1$ to n

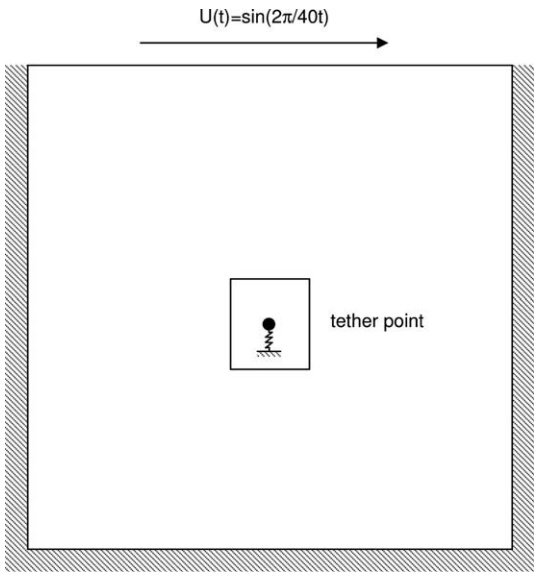

Fig. 6. A driven cavity FSI model with an immersed solid tethered at the center.

$$h_{jj} = r, \quad p_j = c_j b_j, \quad \text{and} \quad p_{j+1} = -s_j b_j. \tag{4.47}$$

Finally, the termination criteria of the GMRES iteration will rest at the absolute value of b_{n+1} in comparison with a given error ϵ. If $|b_{n+1}| < \epsilon$, the solution vector $\Delta\mathbf{\Theta}$, or rather $\Delta\mathbf{V}$, $\Delta\mathbf{P}$, and $\Delta\mathbf{P}^s$ is expressed as

$$\Delta\mathbf{\Theta}^{k,n} = \Delta\mathbf{\Theta}^{k,0} + \sum_{i=1}^{n} y_i \mathbf{q}^i, \text{ or } \begin{bmatrix} \Delta\mathbf{V} \\ \Delta\mathbf{P} \\ \Delta\mathbf{P}^s \end{bmatrix} = \Delta\mathbf{\Theta}^{k,0} + \sum_{i=1}^{n} y_i \mathbf{q}^i. \tag{4.48}$$

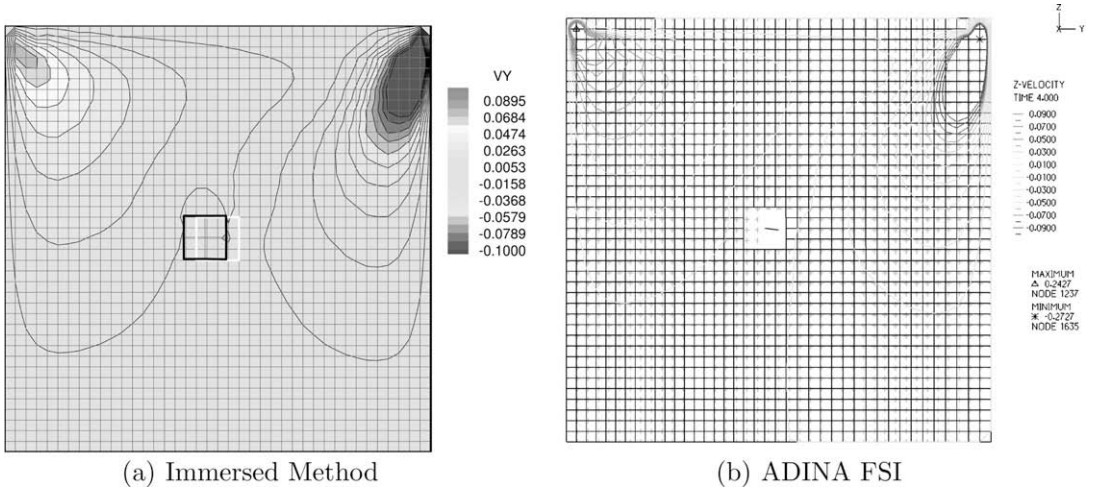

Fig. 7. Snapshots of results from the immersed continuum method and the ADINA FSI solver.

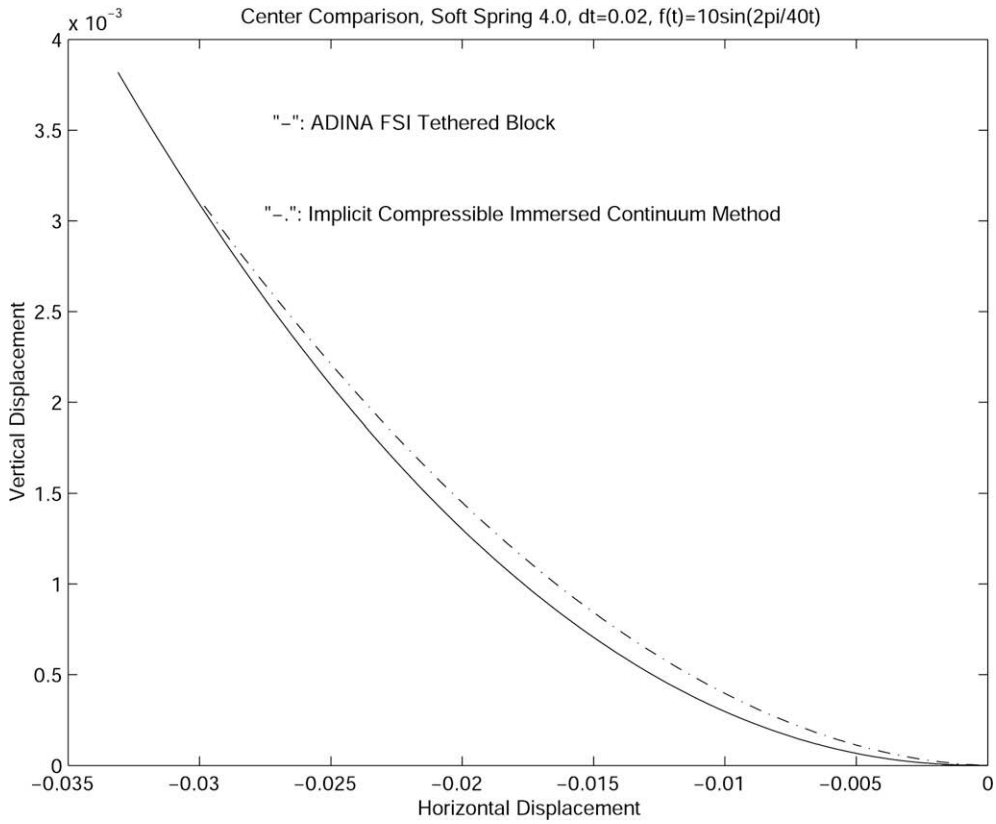

Fig. 8. Comparison of trajectories of the center of the tethered block.

As a final remark, if the initial guess $\Delta\Theta^{k,0}$ does not produce a good estimate within a sufficiently small Krylov subspace $\mathbf{K}^n$. $\Delta\Theta^{k,n}$ will be introduced as an updated initial guess and the GMRES iteration procedure will continue until a solution with the desired accuracy is obtained.

5. Numerical examples

Recently, some breakthroughs have been made in the development of finite element formulations for the immersed boundary/continuum methods. In addition, a preliminary formulation for beams with both bending and torsional moments has been developed [14]. In this paper, we employ a series of driven cavity problems with immersed solids to test various immersed finite element formulations. The key attribute of these series of driven cavity problems is duality of incompressible/compressible issues. Suppose the immersed solid is incompressible, the surrounding fluid must be incompressible. However, if the immersed solid is compressible, the surrounding fluid is still capable of volume change as long as the net system volume is preserved. Because the overall fluid and solid system has a fixed volume, if we use the pseudo compressible viscous fluid model coupled with compressible solids, the results should be similar to incompressible viscous fluid model coupled with incompressible solids if bulk moduli are sufficiently large.

In order to compare immersed methods with traditional mesh adaptive solution procedures, we start with a 1×1 driven cavity model with a 0.1×0.1 immersed solid in the center as shown in Fig. 1. In the immersed continuum method, the background fluid mesh for the entire cavity which includes the space occupied by the immersed solids consists of 20×20 $9/4c$ mixed finite elements as illustrated in Fig. 2. A typical immersed solid is also represented by $9/4c$ mixed finite elements. To match with the compressibility of the immersed solid, we introduce a slightly compressible fluid model with a bulk modulus $2.1e6$ and a viscosity of 1. Since we use the implicit compressible immersed continuum method, it would be feasible to assign stiff springs (4000) to tether all boundary points of the immersed solid as shown in Fig. 3 to mimic an immersed solid fixed in the center as shown in Fig. 1. In addition, a more general case as shown in Fig. 6 with the immersed solid tethered at the center point is also considered. In all three cases, the immersed solid is represented with a Mooney–Rivilin material model with density $\rho_s = 2$, bulk modulus $1e7$, and two additional material constants $C_1 = 40$ and $C_2 = 20$.

For the comparison of fixed immersed solid, we compare the velocity components of the fluid grid point $(0.5, 0.7)$ between the top surface of the cavity and the immersed solid. With the same time step size, as shown in Figs. 4 and 5, the results from the implicit compressible immersed continuum method and the ADINA FSI solver are very close. Considering the fact that these results are derived from two completely different approaches with entirely different meshes, these comparisons are very assuring. Moreover, for the case with the center of the immersed solid tethered with a soft spring, despite

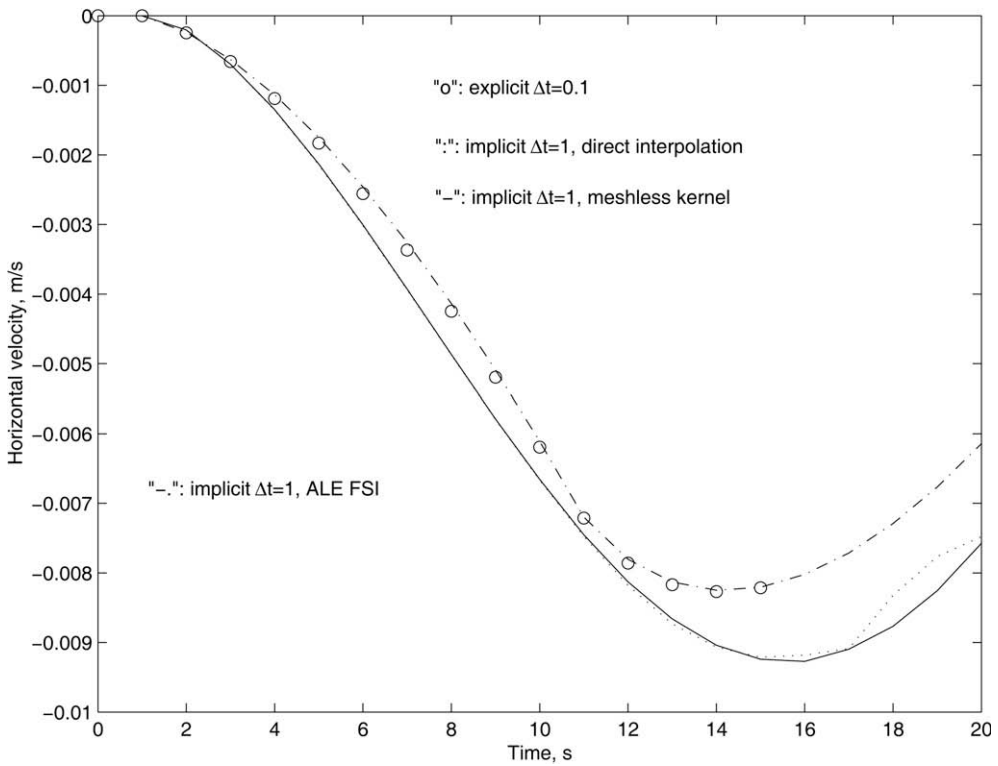

Fig. 9. A comparison of horizontal velocity derived from the traditional ALE formulation and the immersed methods.

the difference of the fluid mesh shown in Fig. 7, the trajectories of the block center derived from the immersed continuum method and the ADINA FSI solver do match well with each other as depicted in Fig. 8. In Fig. 7, the original and current mesh distributions are both depicted along with ADINA results. In the plotting stage, we split each 9-node element into four 4-node element. As a result, the velocity mesh will be two times denser than the pressure mesh. The construction of this mesh demonstrates the philosophical difference between the immersed boundary/continuum methods and the traditional ALE

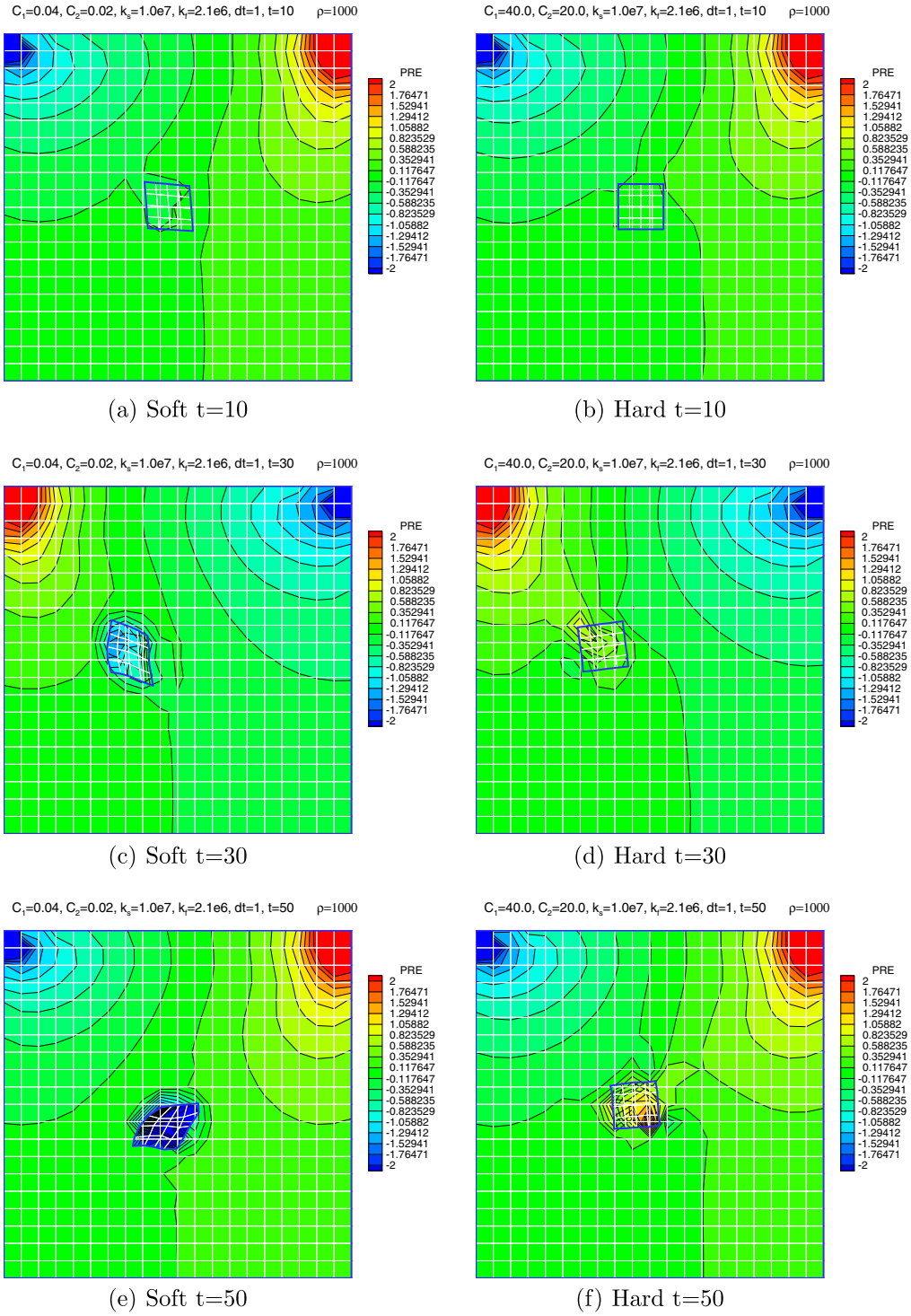

(a) Soft t=10 (b) Hard t=10

(c) Soft t=30 (d) Hard t=30

(e) Soft t=50 (f) Hard t=50

Fig. 10. Pressure snapshots of a driven cavity FSI problem with one immersed deformable solid.

type of modeling approaches. In the immersed continuum method, the solid mesh is right on top of the background fluid mesh, whereas in the ALE formulation, the solid mesh is surrounded by the fluid mesh with a different mesh density. It is not difficult to identify the key advantage of the immersed boundary/continuum methods namely a fixed background fluid mesh for this type of FSI problems.

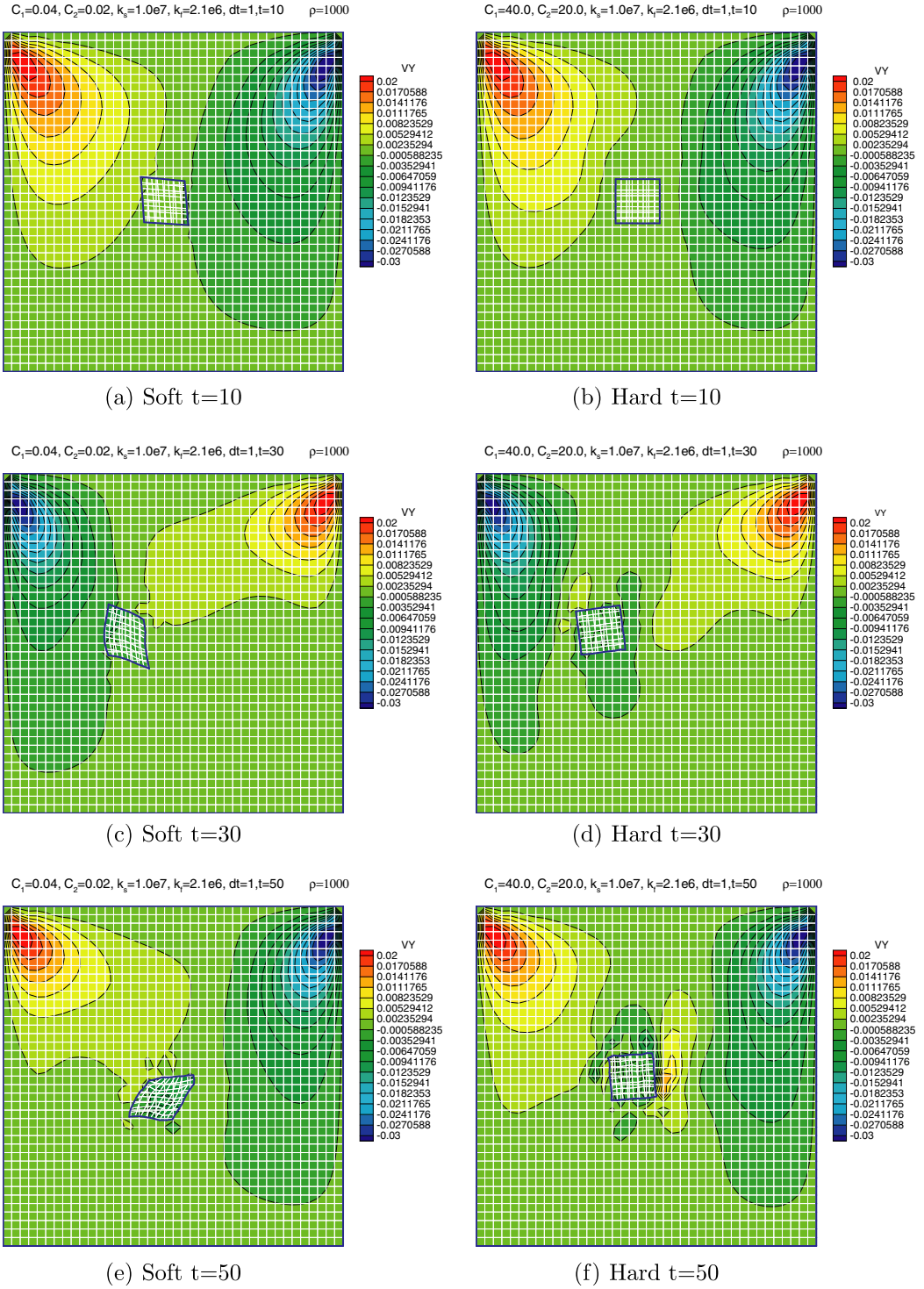

(a) Soft t=10 (b) Hard t=10

(c) Soft t=30 (d) Hard t=30

(e) Soft t=50 (f) Hard t=50

Fig. 11. Vertical velocity snapshots of a driven cavity FSI problem with one immersed deformable solid.

To avoid the overlap of the mesh for the immersed solid and the background fluid mesh, we also alter slightly the dimension of the immersed solid. In the second series of tests, the immersed solid has the dimension of 0.13×0.13. To compare the dynamical behaviors, the top shear velocity of the cavity is set as $0.1\sin(2\pi/40t)$. The deformable solid is situated initially in the center of the cavity with zero velocity. The submerged solid is made of a compressible rubber material with the material constant $\kappa_s = 1e7$ and the density $\rho_s = 1000$. For hard solids we use $C_1 = 40$ and $C_2 = 20$; whereas for soft solids we use

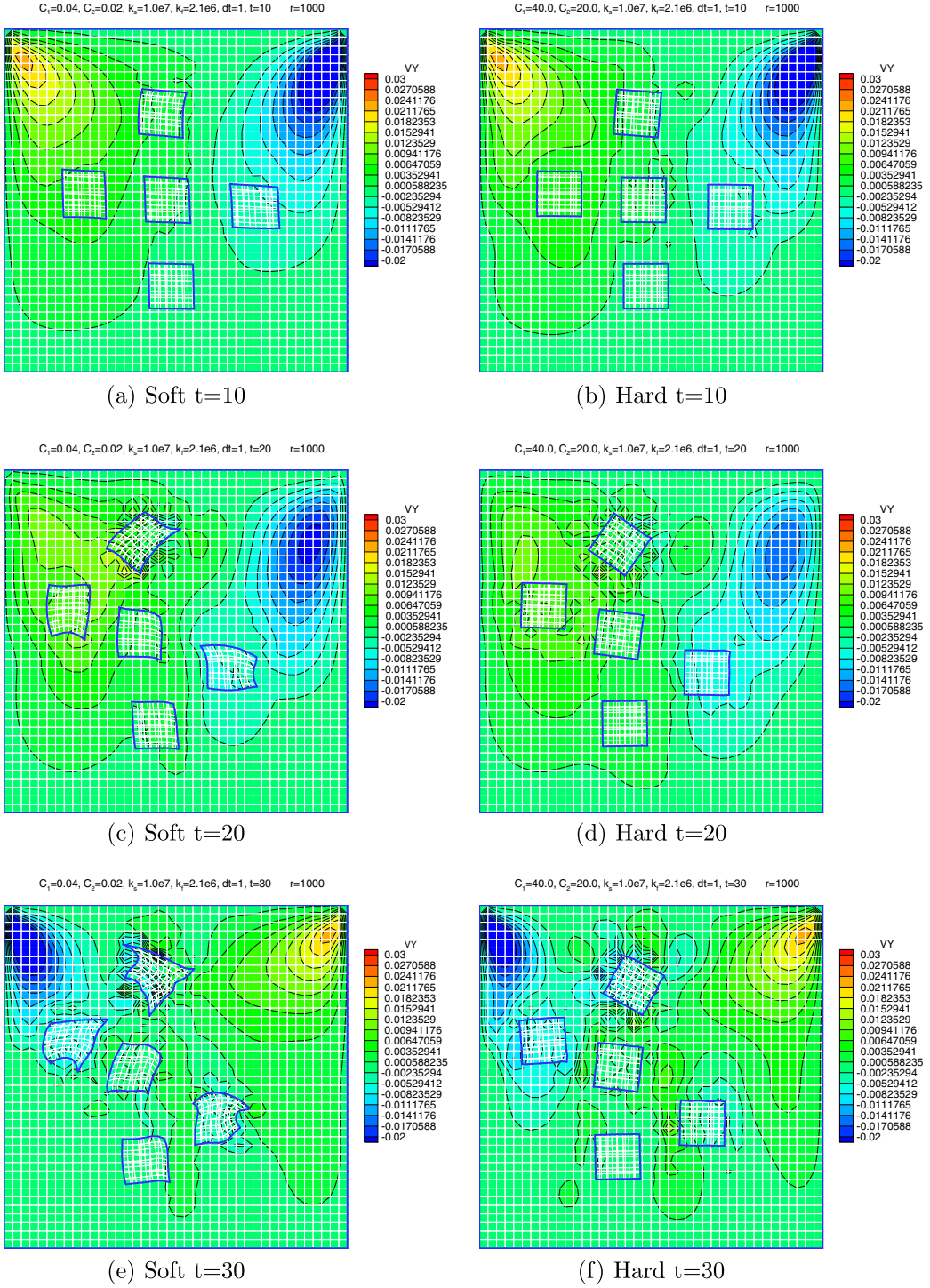

(a) Soft t=10 (b) Hard t=10

(c) Soft t=20 (d) Hard t=20

(e) Soft t=30 (f) Hard t=30

Fig. 12. Vertical velocity snapshots of a driven cavity FSI problem with five immersed deformable solids.

$C_1 = 0.04$ and $C_2 = 0.02$. The case with hard solids resembles the same driven cavity problem with immersed rigid bodies. In addition, the viscous fluid is also represented with compressible model with a constant wave speed. In this case, we have the dynamic viscosity $\mu = 1$, the bulk modulus $\kappa_f = 2.1e6$, and the density $\rho_f = 1000$.

For the case with one immersed square solid, as long as the immersed solid does not move and deform significantly, it is still possible to solve this fluid–solid system with traditional modeling techniques such as the arbitrary Lagrangian–Eulerian

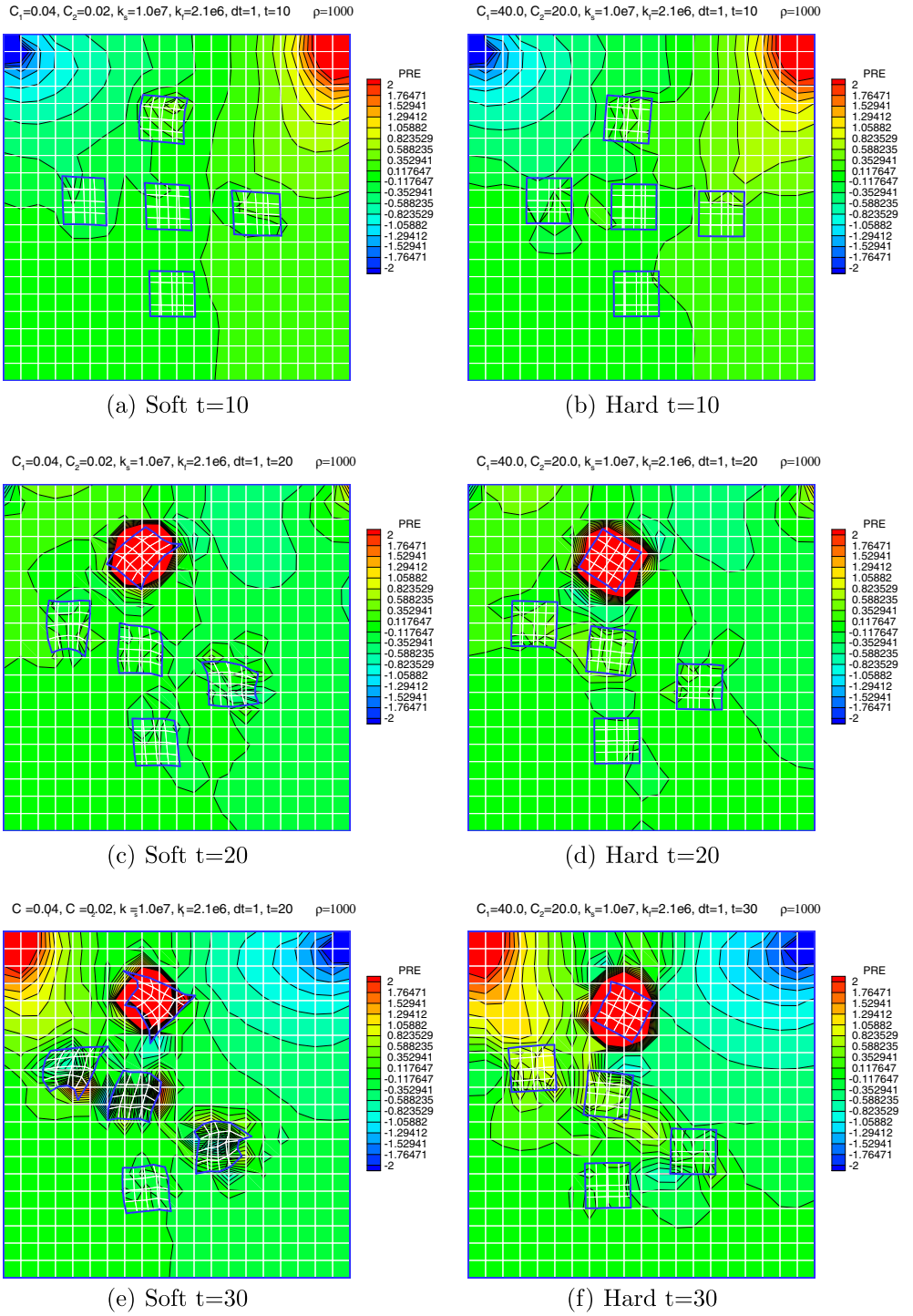

(a) Soft t=10 (b) Hard t=10

(c) Soft t=20 (d) Hard t=20

(e) Soft t=30 (f) Hard t=30

Fig. 13. Pressure snapshots of a driven cavity FSI problem with five immersed deformable solids.

(ALE) formulation. As shown in Fig. 9, even with the coarse mesh used, the implicit immersed continuum method with high-order mixed elements provides reasonable results comparable to reference solutions. It is very important to point out that the discretized delta function provides the possibility of linking the immersed solid node with the surrounding fluid nodes as done in meshless finite element methods. However, as stated in Ref. [3], the immersed solid node can also be restricted to communicate with the very finite element for the background fluid domain. As long as the virtual power input to the surrounding fluid is preserved, the concept of immersed methods will stay the same. This procedure is the same as the standard finite element procedure to distribute concentrated forces and to interpolate displacement/velocity within the element. Whether or not this procedure is as efficient as the meshless type of communication depends very much on the search algorithm for the purpose of locating the immersed solid node.

The pressure and the vertical velocity distributions at different time stations are depicted in Figs. 10 and 11. For soft immersed solids, the initial shear force of the driven cavity problem causes an obvious shear deformation; whereas for hard immersed solids, rigid body like translations and rotations are observed. A side benefit of this implicit compressible immersed continuum method is the volume preservation of the immersed solid. In this case, for both soft and hard solids, the material is almost incompressible with a high bulk modulus. Although this implicit matrix-free Newton–Krylov solution scheme is not very fast, the procedure is not extremely time consuming or prohibitive to carry out for a typical laptop. By choosing the proper preconditioner, the inner GMRES iteration can be mininized to two to three steps while the outer Newton iteration still depends on how close to the solution the initial guess is. In addition, no spatial oscillation and checkerboard pressure bands are observed. Of course, the proposed description can be used for refined meshes. However, as one of the main messages, we must point out that in engineering practice, before a large number of finite elements are used, it is always beneficial to employ coarse meshes with high-order elements to obtain a reasonable estimation of complicated problems.

The benefit of the immersed methods is clear for the case with five immersed solids. For this case, it is no longer feasible to use the ALE formulation, whereas it is a simple task to add a few more deformable solids in the immersed continuum method. In Fig. 12, vertical velocity distributions are shown within the same ranges for both soft and hard solids as well as the previous cases. It is interesting to notice the fine scale fluid motions surrounding the moving solid. Moreover, for soft solids, the shear effects on top of the driven cavity are much more prominent in this particular case. Fig. 13 shows the pressure distributions for both soft and hard solid cases. The important feature of this series of pictures is a significant positive pressure near the top solid around $t = 20$ seconds. Notice that these solutions are converged solutions within a specified error range, in this case 10^{-4}. This type of information is valued in the design of manufacturing processes involving complex fluid–solid mixtures.

6. Conclusions

In immersed methods, in order to satisfy energy conservation, namely, the energy input to the fluid domain from the immersed solid is the same as that from the equivalent body force, the same delta function must be used in both the distribution of the resultant nodal force and the interpolation of the solid velocity based on the surrounding fluid velocities. In fact, the key treatment in the immersed boundary/continuum methods can be viewed as the synchronization of the fluid motion with the solid motion within the immersed solid domain Ω_s, namely,

$$\mathbf{v}^s = \mathbf{v}^f. \tag{6.49}$$

The constraint of Eq. (6.49) introduces the (distributed) Lagrange multiplier as the equivalent body force. In this case, the equivalent body forces can be directly calculated along with independent fluid and solid velocity vectors. Of course, such a procedure will introduce a set of new unknowns equal to the number of velocity unknowns for solids. The early success of immersed finite element formulations for the immersed methods is only the beginning of this type of modeling treatment for complex FSI systems. Recent mathematical studies and extensions to electrokinetics and mass and heat transfers can also be found in Refs. [15,28].

Acknowledgment

The supports from NSF (DMI-0503652 and BES-0503649) and ASEE Summer Faculty Fellowship through AFRL are greatly acknowledged.

References

[1] W. Bao, X. Wang, K.J. Bathe, On the Inf-Sup condition of mixed finite element formulations for acoustic fluids, Mathematical Models and Methods in Applied Sciences 11 (2001) 883–901.
[2] D. Boffi, L. Gastaldi, A finite element approach for the immersed boundary method, Computers and Structures 81 (2003) 491–501.
[3] D. Boffi, L. Gastaldi, L. Heltai, On the CFL condition for the finite element immersed boundary method, Computers and Structures 85 (2007) 775–783.
[4] D. Boffi, L. Gastaldi, L. Heltai, C.S. Peskin, On the hyperelastic formulation of the immersed boundary method, Computer Methods in Applied Mechanics and Engineering 197 (2008) 2210–2231.
[5] J. Chessa, T. Belytschko, The extended finite element method for two-phase fluids, Journal of Applied Mechanics 70 (2003) 10–17.
[6] C.S. Peskin, The immersed boundary method, Acta Numerica 11 (2002) 479–517.
[7] D.A. Knoll, D.E. Keyes, Jacobian-free Newton–Krylov methods: a survey of approaches and applications, Journal of Computational Physics 193 (2004) 357–397.

[8] E.P. Newren, A.L. Fogelson, R.D. Guy, R.M. Kirby, Unconditionally stable discretizations of the immersed boundary equations, Journal of Computational Physics 222 (2007) 702–719.
[9] M. Gay, L.T. Zhang, W.K. Liu, Stent modeling using immersed finite element method, Computer Methods in Applied Mechanics and Engineering 195 (2005) 4358–4370.
[10] G.J. Wagner, N. Moës, W.K. Liu, T.B. Belytschko, The extended finite element method for rigid particles in stokes flow, International Journal for Numerical Methods in Engineering 51 (2001) 293–313.
[11] R. Glowinski, T.W. Pan, T.I. Hesla, D.D. Joseph, J. Périaux, A fictitious domain approach to the direct numerical simulation of incompressible viscous flow past moving rigid bodies: application to particulate flow, Journal of Computational Physics 169 (2001) 363–426.
[12] A. Huerta, W.K. Liu, Viscous flow with large free surface motion, Computer Methods in Applied Mechanics and Engineering 69 (1988) 277–324.
[13] D. Kay, D. Loghin, A. Wathen, A preconditioner for the steady-state Navier–Stokes equations, SIAM Journal on Scientific Computing 24 (1) (2002) 237–256.
[14] S. Lim, A. Ferent, X. Wang, C.S. Peskin, Dynamics of a closed rod with twist and bend in fluid, SIAM Journal on Scientific Computing 31 (2008) 273–302.
[15] Y. Liu, W.K. Liu, T. Belytschko, N. Patankar, A.C. To, A. Kopacz, J.H. Chung, Immersed electrokinetic finite element method, Computer Methods in Applied Mechanics and Engineering 71 (2007) 379–405.
[16] M.D. Tidriri, Preconditioning techniques for the Newton–Krylov solution of compressible flows, Journal of Computational Physics 132 (1997) 51–61.
[17] D. Sulsky, J.U. Brackbill, A numerical method for suspension flow, Journal of Computational Physics 96 (1991) 339–368.
[18] T. Sussman, K.J. Bathe, A finite element formulation for nonlinear incompressible elastic and inelastic analysis, Computers and Structures 26 (1/2) (1987) 357–409.
[19] T. Belytschko, Fluid–structure interaction, Computers and Structures 12 (1980) 459–469.
[20] T.E. Tezduyar, Finite element methods for flow problems with moving boundaries and interfaces, Archives of Computational Methods in Engineering 8 (2001) 83–130.
[21] T.J.R. Hughes, L.P. Franca, M. Balestra, A new finite element formulation for computational fluid dynamics: V. Circumventing the Babuška–Brezzi condition: A stable Petrov–Galerkin formulation of the Stokes problem accommodating equal-order interpolations, Computer Methods in Applied Mechanics and Engineering 59 (1986) 85–99.
[22] R. Van Loon, P.D. Anderson, F.N. Van de Vosse, S.J. Sherwin, Comparison of various fluid–structure interaction methods for deformable bodies, Computers and Structures 85 (2006) 833–843.
[23] X. Wang, From immersed boundary method to immersed continuum method, International Journal for Multiscale Computational Engineering 4 (2006) 127–145.
[24] X. Wang, An iterative matrix-free method in implicit immersed boundary/continuum methods, Computers and Structures 85 (2007) 739–748.
[25] X. Wang, Fundamentals of Fluid–Solid Interactions-Analytical and Computational Approaches, Elsevier Science, 2008.
[26] X. Wang, K.J. Bathe, Displacement/pressure based finite element formulations for acoustic fluid–structure interaction problems, International Journal for Numerical Methods in Engineering 40 (1997) 2001–2017.
[27] X. Wang, W.K. Liu, Extended immersed boundary method using FEM and RKPM, Computer Methods in Applied Mechanics and Engineering 193 (2004) 1305–1321.
[28] W.K. Liu, D.W. Kim, S. Tang, Mathematical foundations of the immersed finite element method, Contemporary Mathematics 193 (2006) 1–12.
[29] W.K. Liu, S. Jun, Y.F. Zhang, Reproducing kernel particle methods, International Journal for Numerical Methods in Fluids 20 (1995) 1081–1106.
[30] W.K. Liu, Y. Liu, D. Farrell, L. Zhang, X. Wang, Y. Fukui, N. Patankar, Y. Zhang, C. Bajaj, X. Chen, H. Hsu, Immersed finite element method and its applications to biological systems, Computer Methods in Applied Mechanics and Engineering 195 (2006) 1722–1749.
[31] W.K. Liu, D.C. Ma, Computer implementation aspects for fluid–structure interaction problems, Computer Methods in Applied Mechanics and Engineering 31 (1982) 129–148.
[32] W.K. Liu, T.B. Belytschko, H. Chang, An arbitrary Lagrangian–Eulerian finite element method for path-dependent materials, Computer Methods in Applied Mechanics and Engineering 58 (1986) 227–245.
[33] Z. Yu, A DLM/FD method for fluid/flexible-body interactions, Journal of Computational Physics 207 (2005) 1–27.
[34] L. Zhang, A. Gerstenberger, X. Wang, W.K. Liu, Immersed finite element method, Computer Methods in Applied Mechanics and Engineering 193 (2004) 2051–2067.
[35] L. Zhang, G.J. Wagner, W.K. Liu, Modeling and simulation of fluid structure interaction by meshfree and FEM, Communications in Numerical Methods in Engineering 19 (2003) 615–621.